Iranian Journal of Catalysis 10(2), 2020, 91-99

IRANIAN JOURNAL OF CATALYSIS

Eco-friendly preparation and characterization of $CuMn_2O_4$ nanoparticles with the green capping agent and their photocatalytic and photovoltaic applications

Ali Sobhani-Nasab[a,*], Mohammad Eghbali-Arani[b], Seyed Mostafa Hosseinpour-Mashkani[a], Farhad Ahmadi[c], Mehdi Rahimi-Nasrabadi[d,e], Vahid Ameri[f]

[a]*Young Researchers and Elite Club, Arak Branch, Islamic Azad University, Arak, Iran.*

[b]*Department of Physics, University of Kashan, Kashan, Iran.*

[c]*Department of Medicinal Chemistry, School of Pharmacy-International Campus, Iran University of Medical Sciences, Tehran, Iran.*

[d]*Chemical Injuries Research Center, Baqiyatallah University of Medical Sciences, Tehran, Iran.*

[e]*Department of Chemistry, Faculty of Pharmacy, Baqiyatallah University of Medical Sciences, Tehran, Iran.*

[f]*Department of Physics, Faculty of Science, University of Hormozgan, Bandar-Abbas, Iran.*

Received 9 January 2018; received in revised form 3 August 2018; accepted 7 August 2018

ABSTRACT

In this study, copper manganese oxide ($CuMn_2O_4$) nanoparticles were successfully synthesized by a simple sol-gel technique in the presence of lactose as the green capping agent. The lactose concentration effect on the crystalline size and magnetic properties of final products were systematically investigated. The structural, morphological, magnetic, and optical properties of as-obtained products were examined by techniques such as the Fourier transform infrared (FT-IR) spectroscopy, energy dispersive X-ray spectroscopy (EDX), X-ray diffraction (XRD), scanning electron microscopy (FESEM), vibrating-sample magnetometer (VSM) and UV–Vis diffuse reflectance spectroscopy. SEM and VSM results show that lactose concentrations play an important role in the magnetic properties and morphology of $CuMn_2O_4$ nanoparticles. Degradation of type of dye (Rhodamine B = Rh B and Methyl orange = MO) under ultraviolet light was examined to assess the feasibility of using $CuMn_2O_4$ for photocatalytic activities. To demonstrate the possibility of developing an inexpensive solar cell, FTO/TiO_2/$CuMn_2O_4$/Pt-FTO, the $CuMn_2O_4$ paste was put on the top of the TiO_2 through the doctor blade technique.

Keywords: *$CuMn_2O_4$, Nanoparticles, Green capping agent, Photocatalysis, Sol-gel technique.*

1. Introduction

Nowadays, semiconductor nanomaterials have been extensively studied because of their high efficiency photocatalytic properties [1-5]. Spinels with general formula of AB_2O_4 are very well known materials due to their flexibility in incorporating various ions into their crystal structure. The magnetic spinel ferrites have been used in electrical engineering such as microwave devices and inductors; while magnetic, electric, thermo electric, and catalyst properties of the copper manganite spinel make it suitable for a wide range of applications [6-8].

*Corresponding author.
Email: ali.sobhaninasab@gmail.com (Ali Sobhani-Nasab)

The multivalent nature of Mn and Cu in $CuMn_2O_4$ structure makes them suitable candidates for engineering applications. Besides, the site orientation of Mn and Cu in $CuMn_2O_4$ has an important role in its properties [9-12]. The potential for $CuMn_2O_4$ as the catalysis education of NO_x with NH_3 at a low temperature and for oxidation of CO at ambient temperature and fore spiratory protection, particularly in the mining industry, attracts a lots of attention [13-15]. The distributions of Cu^{2+} and Mn^{3+} in $CuMn_2O_4$ structure are in tetrahedral and octahedral sites, respectively, which are known as normal spinel structures; the corresponding general formula is written as $A^{tet}B_2{}^{oct}O_4$ [16]. The amounts of Mn^{4+} species and compositional homogeneity cause high activity of this

spinel compound. Hence, in this report, we have presented the preparation of $CuMn_2O_4$ nanoparticles by a simple sol-gel method in the presence of lactose as the green capping agent. Besides, different concentrations of lactose were applied to investigate its impact on the morphology and magnetic properties of final products. For investigation photocatalytic activity of nanoparticles several factors such as various dyes, different light and grain size of $CuMn_2O_4$ nanoparticles were applied. The solar cell property of $CuMn_2O_4$ nanoparticles was investigated.

2. Experimental

2.1. Characterization

Manganese (II) nitrate hydrate, Copper(II) nitrate, lactose, methyl orange (MO) and rhodamine-B (RhB) were purchased from Merck Company and used without further purification. The X-ray diffraction (XRD) pattern was recorded by a Philips-X'PertPro, X-ray diffractometer using Ni-filtered Cu Kα radiation at the scan range of $10<2\theta<80$. Scanning electron microscopy (SEM) images were obtained on LEO-1455VP equipped with an energy dispersive X-ray spectroscopy. The energy dispersive spectrometry (EDS) analysis was studied by the XL30, Philips microscope. The magnetic measurement of sample was carried out in a vibrating sample magnetometer (VSM) (Meghnatis Daghigh Kavir Co.; Kashan Kavir; Iran) at room temperature. Fourier transform infrared (FT-IR) spectra were recorded on Magna-IR, spectrometer 550 Nicolet with 0.125 cm^{-1} resolution in KBr pellets in the range of 400-4000 cm^{-1}. Photocurrent density-voltage (J-V) curve was measured using computerized digital multimeters (Ivium-n-Stat Multichannel potentiostat) and a variable load. A 300 W metal xenon lamp (Luzchem) served as a simulated sun light source, and its light intensity (or radiant power) was adjusted to simulated AM 1.5 radiation at 100 mW/cm with a filter for this purpose. Transmission electron microscope (TEM) images were taken on a JEM-2100 with an accelerating voltage of 200 kV. UV-Vis diffuse reflectance spectroscopy analysis (UV-Vis) was carried out using the Shimadzu UV-Vis scanning spectrometer.

2.2. Synthesis of $CuMn_2O_4$ nanoparticles

In a typical synthesis, in two separate beakers, copper nitrate (1 mmol/mL) (187000 ppm) and manganese nitrate (2 mmol/mL) (356000 ppm) were dissolved in 30 mL of distilled water under stirring, separately, and then was mixed. Afterwards, a 30 mL solution containing different lactose concentration (0.5, 1, 1.5, and 2 mmol/mL) (1 mmol=342000 ppm) was added drop wise into the above mixture solution. The final mixed solution was stirring to remove solvent and form a gel at 90 ℃ for 15 min and 110 ℃ for 10 min, respectively. Finally, the obtained product was calcinated at 800 ℃ for 5 h in a conventional furnace in air atmosphere. The products were characterized by XRD, SEM and TEM. All synthesis conditions are illustrated in Table 1.

2.3. Photocatalytic experimental

The photocatalytic activity of copper manganese oxide was studied in the presence of methyl orange (MO) and rhodamine-B (RhB) aqueous solution as a target pollutant at room temperature. First, 100 mL of MO or RhB solution (25 ppm) and $CuMn_2O_4$ (0.05 g) were placed in a quartz photocatalytic reactor. Then, the above mixture was aerated in a dark space for 30 min to reach adsorption equilibrium. Afterwards, the mixture was placed inside the photoreactor, a reactor in which the quartz vessel was 30 cm away from the UV source, 400 W mercury lamps. Aliquots of the mixture were taken at definite time intervals during the irradiation, centrifuged, and then they were analyzed by a UV-vis spectrometer at 563 and 507 nm, corresponding to the maximum absorption wavelength of RhB and MO, respectively. The decolorization efficiencies (%) of rhodamine B (RhB) and MO using $CuMn_2O_4$ nanoparticles at 70 min are listed in Table 1, they are calculated by the following equation.

$$\text{Degradation\%} = [(C_0\text{-}C)/C_0] \times 100 \quad (\mathbf{1})$$

Where C_0 and C are initial concentration and changed absorbencies of dye after ultraviolet irradiation, respectively.

2.4. Fabrication of FTO/TiO_2/$CuMn_2O_4$/Pt-FTO Cell

First, TiO_2 film was prepared through Electrophoresis deposition (EPD) method in which the cleaned FTO glass as a positive potential (anode) was placed with 3 cm distance with a pure steel mesh as the counter electrode (cathode). Megatek Programmable DC Power Supply (MP-3005D) was used to apply 10 V. The deposition cycle took place on the area of the film was 1×1 cm^2 for 4 times, each time 5s, and at temperature 25 ℃. After deposition, resulted layer was annealed under an air flow at 500 ℃ for 30 min. Electrolyte solution consisted of 120 mg/l of I_2, 48 ml/l of acetone, and 20 ml/l of water. For deposition of $CuMn_2O_4$ powder on the TiO_2, a paste of $CuMn_2O_4$ was initially prepared by mixing and grinding 1 g of $CuMn_2O_4$ nanoparticles with ethanol and water in several steps and then sonicated with ultra-sonic horn (Sonicator 3000; Bandeline, MS 72, Germany) and mixed with terpineol and ethyl cellulose as binders. Afterwards, ethanol and water were removed with a rotary-

evaporator to prepare final $CuMn_2O_4$ paste. In order to make anode electrode, the prepared paste was coated on TiO_2 film by a doctor blade technique and then gradually heated under an air flow at 450 °C for 30 min. Besides, counter-electrode was made from deposition of a Pt solution on FTO glass. Afterwards, this electrode was placed over $TiO_2/CuMn_2O_4$ electrode. Sealing was accomplished by pressing the two electrodes together on a double hot-plate at 110 °C. The redox electrolyte consisting of 0.05 M of LiI, 0.05 M of I_2, and 0.5 M of 4-tert-butylpyridine in acetonitrile as a solvent was introduced into the cell through one of the two small holes drilled in the counter electrode. Finally, these two holes were sealed by a small square of sealing sheet and characterized by I-V test.

3. Results and Discussion

The XRD patterns of as-prepared $CuMn_2O_4$ before and after calcination are shown in Fig. 1. The spectrum of bare $CuMn_2O_4$ sample shows a series of diffraction peaks at the position of 18.32° ((102) line), 29.18° ((111) line), 36.18° ((110) line), and 43.63° ((211) line) which is in good agreement with the standard JCPDS file of $CuMn_2O_4$ nanoparticles cubic phase (JCPDS No. 74-2422) shows in Figs. 1 b-e (samples 1-4).

No other crystalline phases were detected in the calcined product. From XRD data, the crystallite diameter (D_c) of $CuMn_2O_4$ nanoparticles obtained from sample 1-4 after calcinations were calculated to be 25, 21, 18, and 11 nm using the Scherer equation [17]:

$$D_c = K\lambda/\beta\cos\theta \qquad (2)$$

Where β is the breadth of the observed diffraction line at its half intensity maximum, K is the so-called shape factor, which usually takes a value of about 0.9, and λ is the wavelength of X-ray source used in XRD. To examine the concentration effect of lactose on the morphology of $CuMn_2O_4$ after calcinations four experiments were performed, as shown in Figs. 2 a-d. In the presence of 0.5 mmol of lactose (Fig. 2 a), the products mainly consist of agglomeration nanoparticles. Further increasing in the lactose concentration to 1, 1.5, and 2 mmol causes particle size and amount of agglomeration to decrease, as shown in Figs. 2 b-d, respectively. Therefore, based on Figs. 2 a-d, an optimum lactose concentration is 2 mmol. The optimum molar ratio of lactose (2 mmol) is the maximum amount of lactose needed to attach metal ions under the assumption that metal ions substitute the hydrogen from -OH groups in the lactose molecule. In the presence of 2 mmol lactose, the lactose molecules as the capping agent could orient in different directions, hence, the obtained particles had little opportunity for

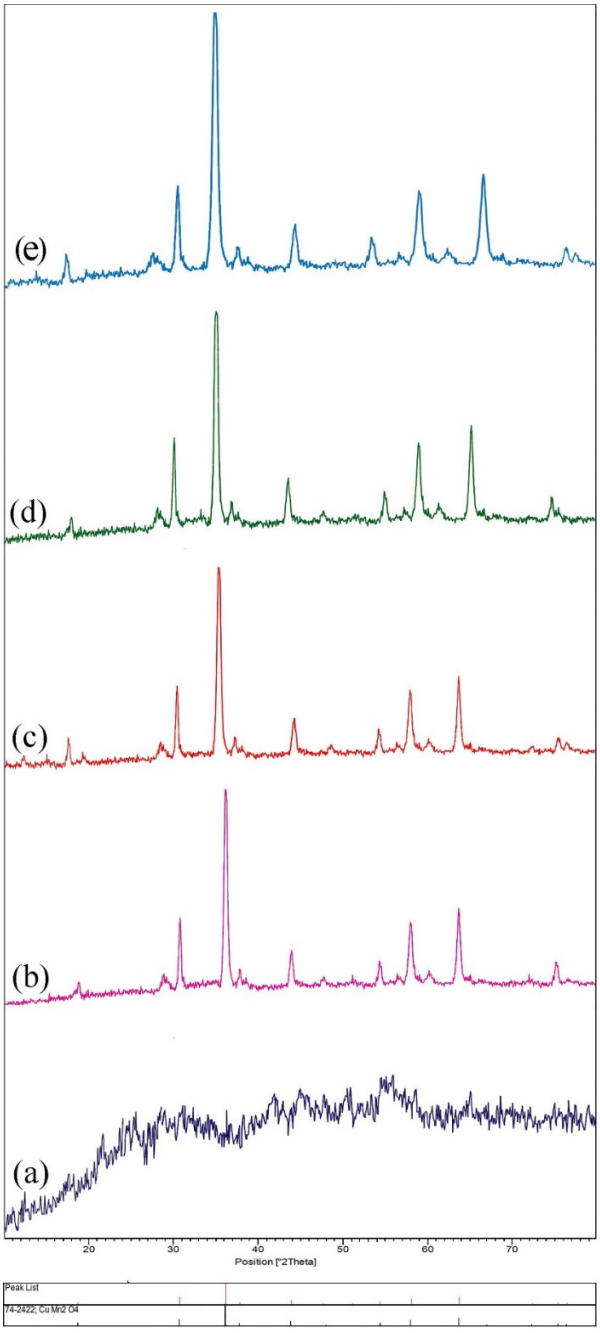

Fig. 1. XRD patterns of $CuMn_2O_4$ nanoparticles (a) sample 1 before calcination and after calcination (b) sample 1 (c) sample 2 (d) sample 3 (e) sample 4.

connection together and become agglomerate. Due to the benefit from lactose as the capping agent in this study, EDS analysis measurement was used to investigate the chemical composition and purity of $CuMn_2O_4$ nanoparticles (sample 4), as shown in Fig. 3. According to Fig. 3, sample 4 consists of Cu, Mn, and O elements. Furthermore, neither N nor C signals were detected in the EDS spectrum, which means the product is pure and free of any surfactant or impurity.

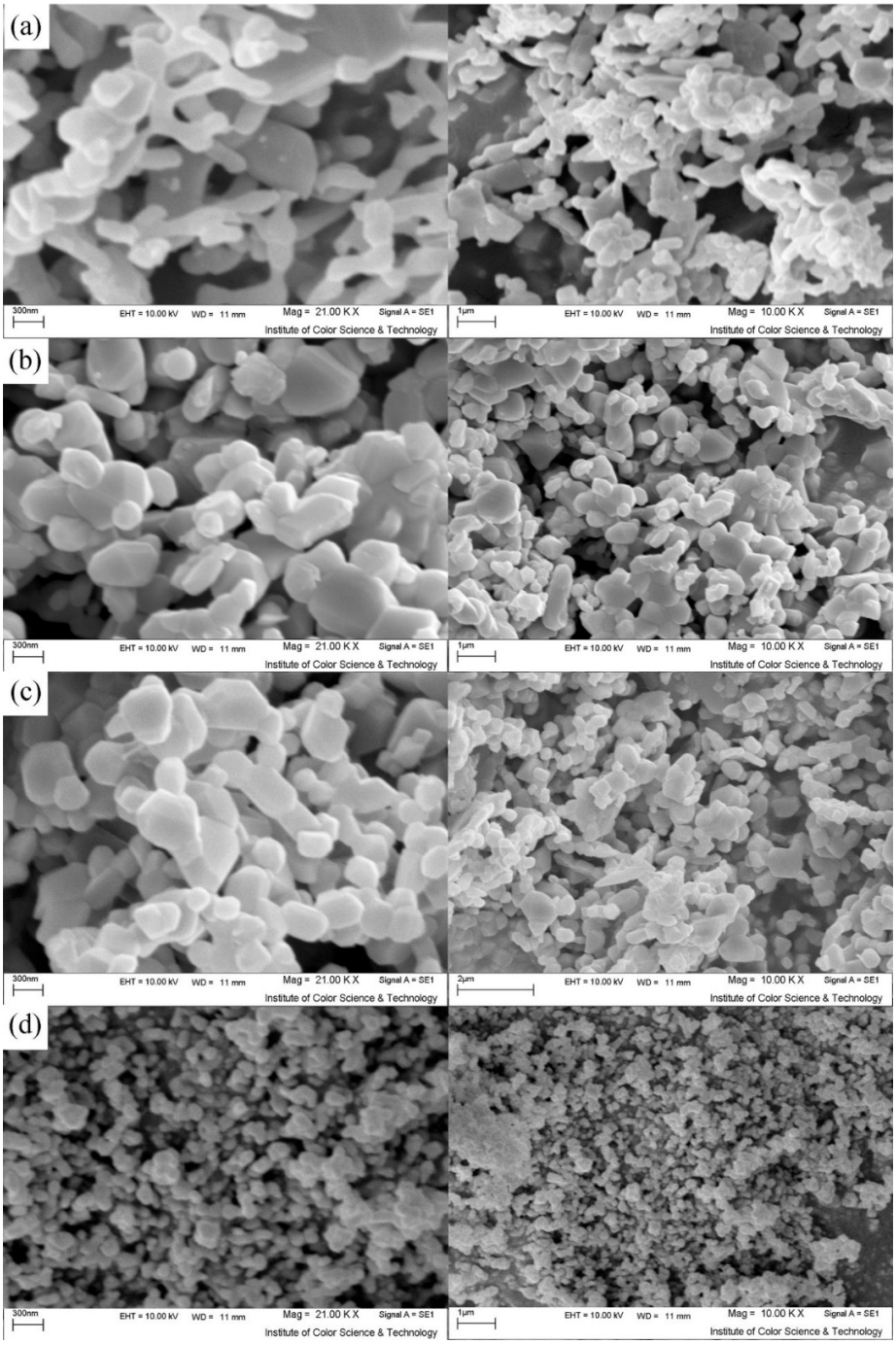

Fig. 2. SEM images of calcined $CuMn_2O_4$ nanoparticles (a) sample 1 (b) sample 2 (c) sample 3 (d) sample 4.

Magnetic properties of $CuMn_2O_4$ (samples 1-4) after calcination at 800 ℃ were investigated through the vibration sample magnetometer (VSM), as shown in Fig. 4. Based on Fig. 4, $CuMn_2O_4$ nanoparticles exhibit paramagnetic to superparamagnetic behavior from sample 1 to sample 4 thanks to its particle size. By increasing the lactose concentration, $CuMn_2O_4$ nanoparticles show a nonlinear magnetization, very thin hysteresis loop, and very small coercively and remanent magnetization. The field dependence of the magnetic materials obeys the following relation (2):

$$M=\chi H \quad (3)$$

where χ is the specific susceptibility. According to Fig. 4 and Table 1, when the lactose concentration increased and the size of $CuMn_2O_4$ nanoparticles decreased, the susceptibility (χ) has been increased.

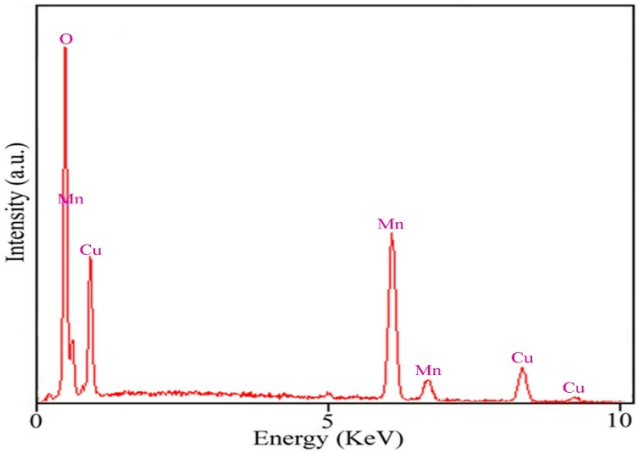

Fig. 3. EDS pattern of calcined $CuMn_2O_4$ nanoparticles (sample 4).

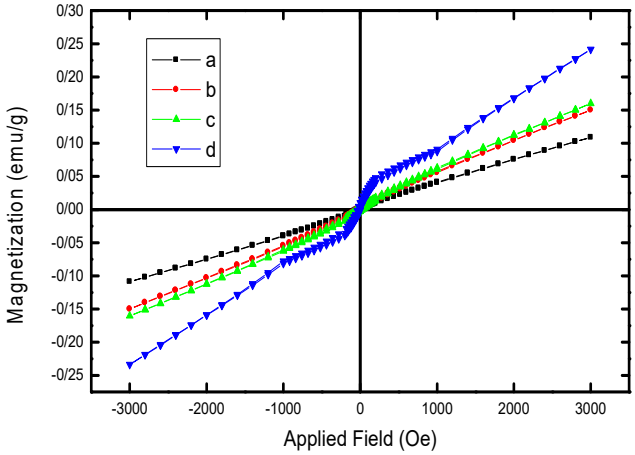

Fig. 4. VSM curves of calcined $CuMn_2O_4$ nanoparticles (a) sample 1 (b) sample 2 (c) sample 3 (d) sample 4.

This is because of different tendencies of nanoparticles for crystallinity by increasing of lactose concentration causing changes to the lattice constant and oxygen parameter of nanoparticles. Originally the bulk of $CuMn_2O_4$ shows an Antiferromagnetic (AFM) behavior. But, here AFM nanoparticles have a pretty weak "paramagnetic" susceptibility in the AFM ordered phase, antiferromagnets do not tend to have a finite magnetization/moment. In nanoscale powders, grains may possess uncompensated moments, though, and there could be paramagnetism due to these. This study shows that superparamagntism appears when the size of crystallines decreases and in sufficiently small nanoparticles [18]. The temperature can randomly flip the direction of magnetic moments tending to be in the average zero. Here the $CuMn_2O_4$ nanoparticles show in, principle, the pretty weak paramagnetic to superparamagnetic behavior. So, eq. 2 is in agreement to 3 curves of Table 1 (sample 1, sample 2, and sample 3). Only sample 4 according to Fig. 4 (blue curve) has a low deviation from eq. 2 because of stronger superparamagnetic behavior (s-shaped). In Table 1, we derived the susceptibility of sample 4 by extrapolation of magnetization curve (by neglecting its manner in very low magnetic field). Indeed, χ is the slope of M vs H.

The diffused reflectance spectrum of the as-prepared $CuMn_2O_4$ nanoparticles (sample 4) is shown in Fig. 5. The fundamental absorption edge in most semiconductors follows the exponential law. Using the absorption data, the band gap was estimated by Tauc's relationship [19-22]:

$$\alpha=\alpha_0 (h\nu-Eg)^n/h\nu \quad (4)$$

where α is absorption coefficient, $h\nu$ is the photon energy, $\alpha 0$ and h are the constants, E_g is the optical band gap of the material, and n depends on the type of electronic transition and can be any value between 0.5 and 3. The energy gap of the $CuMn_2O_4$ nanoparticles (sample 4) is determined by extrapolating the linear portion of the plots of $(\alpha h\nu)^{1/2}$ against $h\nu$ to the energy axis, as shown in Fig. 5.

The E_g value is calculated as 3.2 eV. Fig. 6 a and b shows the FT-IR spectra of $CuMn_2O_4$ nanoparticles (sample 4) before and after washing with methanol, respectively. There are some weak peaks that refer to the presence of lactose impurities such as 3430 cm^{-1} (O-H and N-H group), 2930 and 2870 (C-H stretching vibrations), 1130 (C-O stretching vibrations) [23]. The characterization peaks in Fig. 6 b are 624 cm^{-1} (vibration of atoms intetrahedral oxygen environment; Cu–O at $CuMn_2O_4$) and 527 (vibration of manganese atoms in the octahedral oxygen environment in $CuMn_2O_4$) [24].

Table 1. Reaction conditions for $CuMn_2O_4$ nanoparticles.

Sample No	Temp. (°C)	Lactose conc. (mmol/mL)	Degradation efficiency RhB (%)	Degradation efficiency MO (%)	Susceptibility×10^5 (cm^3/g)	Crystallite Size (nm)
1	800	0.5	76	40	3.8	25
2	800	1	85	-	5.2	21
3	800	1.5	88	-	5.6	18
4	800	2	97	57	9.1	11

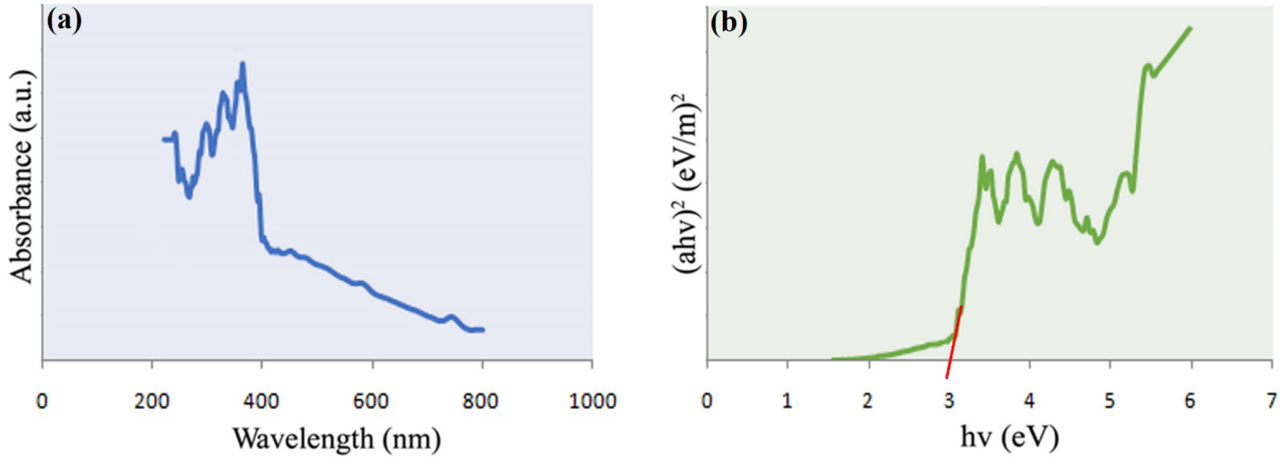

Fig. 5. Diffuse Reflectance Measurement pattern of calcined $CuMn_2O_4$ nanoparticles (sample 4).

To study the morphology and particle size of $CuMn_2O_4$ (sample 4) better, TEM image was taken (Fig. 7). According to Fig. 7, it seems that the morphology of $CuMn_2O_4$ (sample 4) is sphere-like nanoparticles with particle size of ~ 40-50 nm.

The photocatalytic behavior of the $CuMn_2O_4$ nanoparticles calcined at 800 °C (sample No. 1) under UV and visible lights was investigated, as shown in Fig. 8. Photodegradation of RhB under UV irradiation was employed to evaluate the photocatalytic activity of the prepared $CuMn_2O_4$ nanoparticles.

Fig. 8a shows the results of photodegradation of RhB under UV and Vis light with the catalyst, in the presence of the catalyst without UV light, and in the presence of only UV light which are 76, 45, 2 and 4% respectively [24].

Furthermore, Fig. 8b shows the results of photodegradation of MO under UV and Vis light with the catalyst, in the presence of the catalyst without UV light, and in the presence only UV light which are 40, 28, 2 and 4%, respectively [25-33].

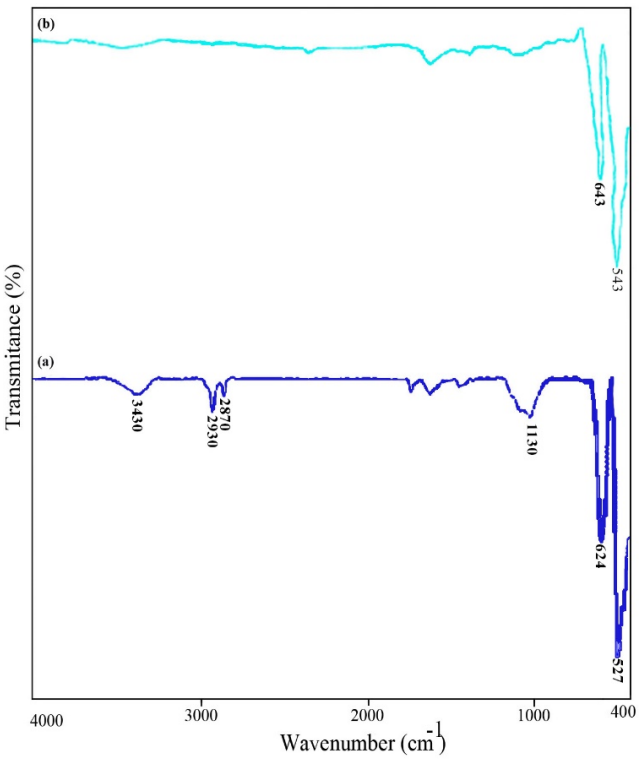

Fig. 6. FT-IR spectra of calcined $CuMn_2O_4$ nanoparticles sample 4 (a) before washing with methanol (b) after washing with methanol.

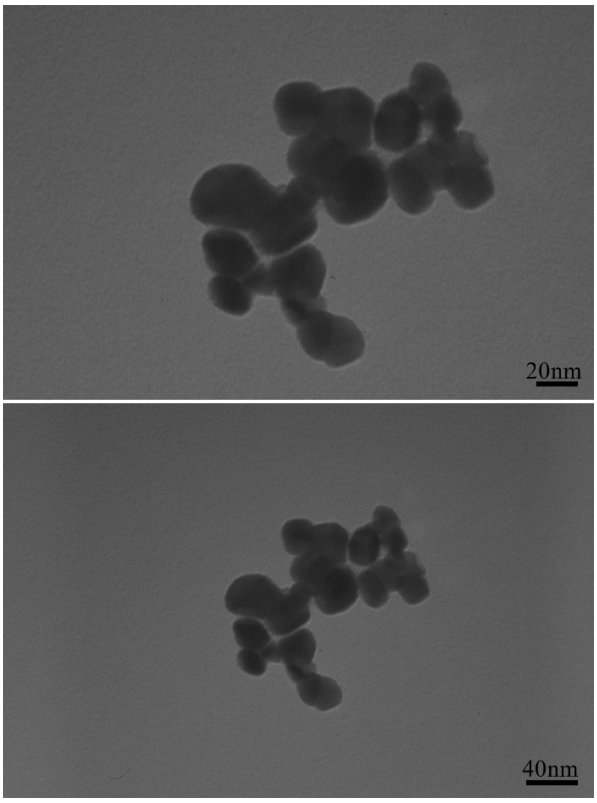

Fig. 7. TEM image of calcined $CuMn_2O_4$ nanoparticles (sample 4).

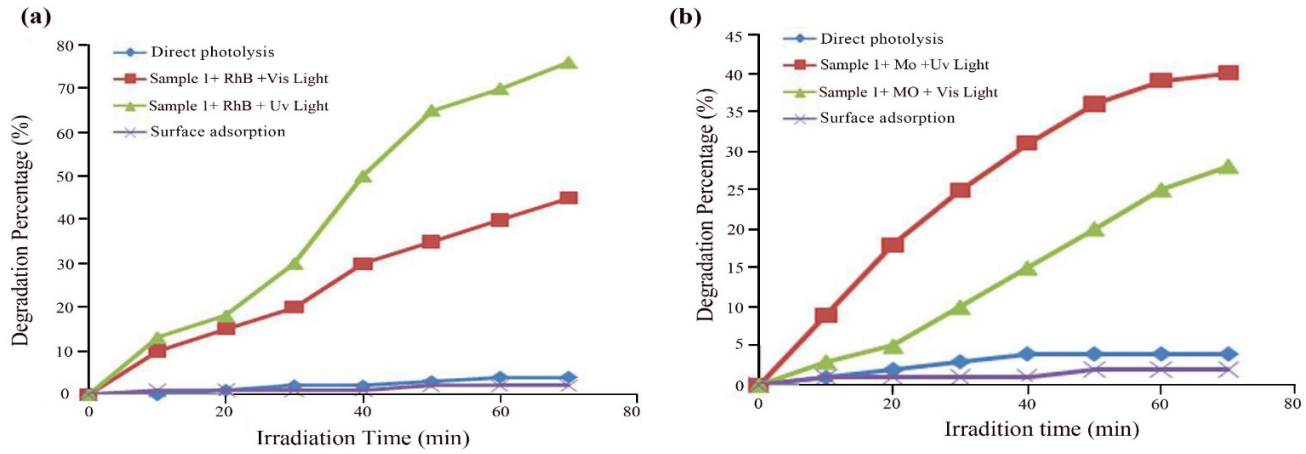

Fig. 8. Photocatalytic degradation of (a) RhB and (b) MO by $CuMn_2O_4$ nanoparticles (samples 1) under Uv and Vis light.

Photocatalytic activities of $CuMn_2O_4$ nanoparticles (sample 1-4) were examined in the presence of MO under UV light, as shown in Fig. 9. In the absence of nanocrystalline $CuMn_2O_4$ no methyl orange was broken down after 70 min. The probable photocatalytic degradation mechanism of dyes in the presence of $CuMn_2O_4$ can be summarized as follows [34-36]:

$$CuMn_2O_4 + h\nu \rightarrow CuMn_2O_4^{\bullet} + e^- + h^+ \quad (5)$$

$$h^+ + H_2O \rightarrow OH^{\bullet} \quad (6)$$

$$e^- + O_2 \rightarrow O_2^{\bullet -} \quad (7)$$

$$OH^{\bullet} + O_2^{\bullet -} + \text{dyes} \rightarrow \text{Degradation products} \quad (8)$$

The methyl orange degradation percentages were about 66, 75, 78, and 96 % after 70 min UV irradiation (samples 1-4 respectively). The effect of various anionic (MO) and cationic (RhB) contaminants on photocatalytic activity of $CuMn_2O_4$ nanoparticles, were studied, as shown in Fig. 10.

Obviously, the photocatalytic behavior of anionic contaminants with a negative charge is lower than cationic contaminant with a positive charge. The percentages of decomposition efficiency for MO and RhB are 60 and 97, respectively. Besides, the whole photocatalytic mechanism is shown in Scheme 1. Furthermore, Ethanediotic acid, 1,2-benzenedicarboxylic acid, benzoic acid, and 4-hydroxybenzoic acid are the results of RhB degradation. I-V characterization of $CuMn_2O_4$ (sample 4) is shown in Fig. 11. The measurement of the current density voltage (I-V) curve for $CuMn_2O_4$ (sample 4) was carried out under the illumination of AM 1.5 (100 mW/cm^2). Device characteristics are as follows: V_{oc}= 0.32 V, J_{sc}= 0.45 mA/cm^2, and FF = 31.5 %.

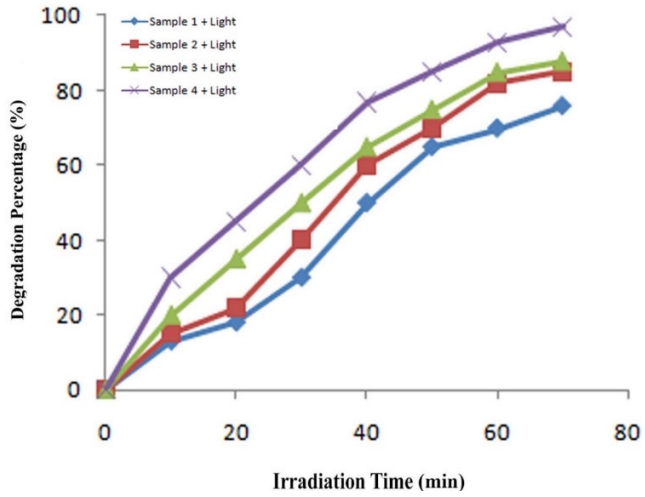

Fig. 9. Photocatalytic degradation of RhB by $CuMn_2O_4$ nanoparticles (samples 1- 4) under ultraviolet light.

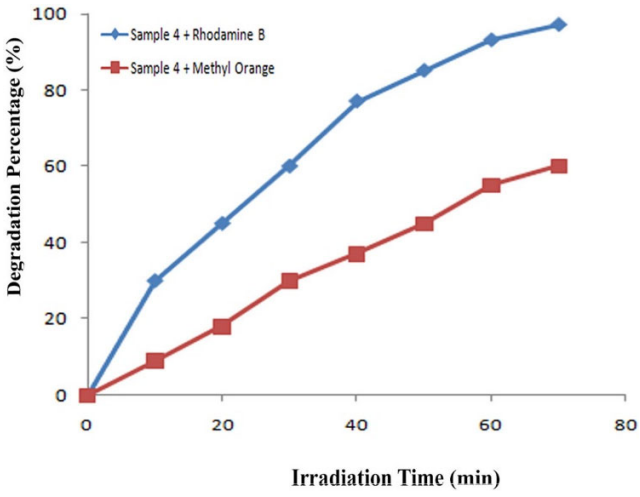

Fig. 10. Photocatalytic degradation of RhB and MO by $CuMn_2O_4$ nanoparticles (samples 4).

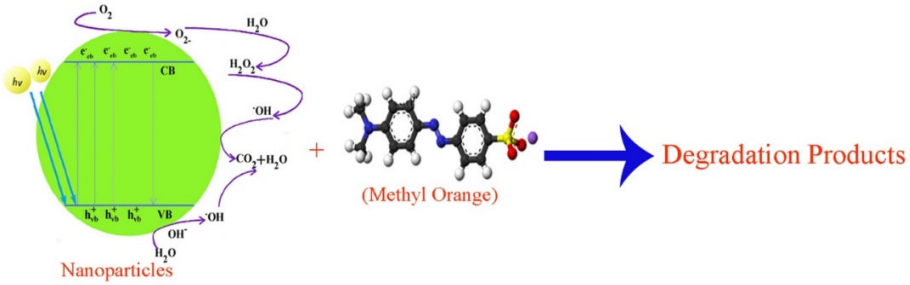

Scheme 1. Photodegradation mechanism of MO over $CuMn_2O_4$ nanoparticles under UV light irradiation

In comparison to other similar works illustrated in Table 2, our method is simple, has low cost, and scale-up route. Besides, to the best of the authors' knowledge, it is the first time that $CuMn_2O_4$ nanoparticles were synthesized in the presence of lactose as the green capping agent and used for degradation of methyl orange under ultraviolet light.

4. Conclusions

In summary, the simple sol-gel method for synthesizing $CuMn_2O_4$ nanoparticles is developed with the aid of lactose as the capping agent. In addition, the effect of lactose concentration on the particle size and magnetic properties were systematically investigated. Applying nanocrystalline $CuMn_2O_4$ as the photocatalyst leads to the maximum 97 % degradation of RhB. Solar cell yield was examined by the constructed electrode as the working electrode through the electrophoresis deposition (EPD) and then studied by the current density voltage (JeV) curve. It was found that FTO/TiO2/$CuMn_2O_4$/Pt-FTO structure had the maximum FF = 31.5 %.

Acknowledgments

Authors are grateful to the council of University of Kashan for providing financial support to undertake this work and Padideh Noavaran Nano Bonyan Company, Iran (Grant number: 785218/2). The authors declare that they have no conflict of interest.

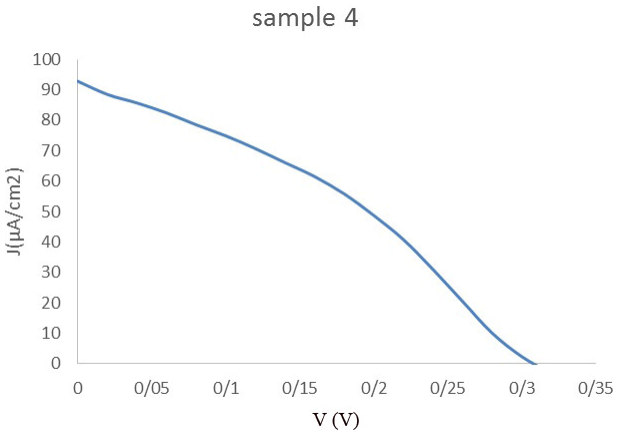

Fig. 11. J-V characterization of calcined $CuMn_2O_4$ nanoparticles calcined (sample 1).

References

[1] H. Wang, F. Wen, X. Li, X. Gan, Y. Yang, P. Chen, Y. Zhang, Sep. Purif. Technol. 170 (2016) 190-198.
[2] P. Sathe, M.T.Z. Myint, S. Dobretsov, J. Dutta, Sep. Purif. Technol. 162 (2016) 61-67.
[3] M.M. Jaffer Sadiq, A. Samson Nesaraj, J. Nanostruct. Chem. 5 (2015) 45–54.
[4] H.S. Wahab, A.A. Hussain, J. Nanostruct. Chem. 6 (2016) 261–274.
[5] H. Zhu, R. Jiang, J. Li, Y. Fu, S. Jiang, J. Yao, Sep. Purif. Technol. 31 (2017) 184-193.
[6] S. Khademolhoseini, J Mater Sci: Mater Electron. 28 (2017) 7899–7904.
[7] J.G. Moyer, D.A. Kukuruznyak, N. Nguyen, M.S. Prowse, F.S. Ohuchi, J. Appl. Phys. 100 (2006) 083504-083509.

Table 2. Comparison of $CuMn_2O_4$ nanoparticles with other similar works.

Method	Precursor	Temp (°C)	Application	Ref.
Co-melting	Cu and Mn metals	1250	—	[21]
Co-precipitation	$Cu(NO_3)_2{\cdot}3H_2O$ and $Mn(NO_3)_2{\cdot}4H_2O$	900	CO_2-selectivity	[22]
Alkaline hydrothermal treatment	$Cu(CH_3COO)_2$ and $Mn(CH_3COO)_2$	12 h stirring and calcined at 500	Catalytic combustion of toluene	[23]
Thermal decomposition	$Cu(NO_3)_2{\cdot}2.5H_2O$, $Mn(NO_3)_2{\cdot}4H_2O$, glycerol, maleic acid, citric acid, ethyl acetoacetate, or nitric acid)	700 for 6 h	Catalysts	[24]

[8] P. Hirunsit, K. Faungnawakij, J. Phys. Chem. C 117 (45) (2013) 23757–23765.
[9] D.P. Shoemaker, J. Li, R. Seshadri, J. Am. Chem. Soc. 131 (2009) 11450-11457.
[10] H. Einaga, A. Kiya, S. Yoshioka, Y. Teraoka, Catal. Sci. Technol. 4 (2014) 3713-3722.
[11] P. Larsson, A. Andersson, Appl. Catal. B 24 (2000) 175–192.
[12] P. Wei, M. Bieringer, L.M.D. Cranswick, A. Petric, J. Mater. Sci. 45 (2010) 1056-1062.
[13] Q. Tang, X. Gong, P. Zhao, Y. Chen, Y. Yang, Appl. Catal. A 389 (2010) 101-107.
[14] E.C. Njagi, H.C. Genuino, C.K. Kingondu, S. Dharmarathna, S.L. Suib, Appl. Catal. A 421 (2012) 154-160.
[15] D. Fang, j. Xie, D. Mei, Y. Zhang, F. He, X. Liu, Y. Li, RSC Adv. 4 (2014) 25540-25552.
[16] Z.R. Tang, S.A. Kondrat, C. Dickinson, J.K. Bartley, A.F. Carley, S.H. Taylor, T.E. Davies, M. Allix, M.J. Rosseinsky, J.B. Claridge, Z. Xu, S. Romani, M.J. Crudace, G.J. Hutchings, Catal. Sci. Technol. 1 (2011) 740-74.
[17] B. Khodadadi, M. Bordbar, Iran. J. Catal. 6 (2016) 37-42.
[18] M. Mozaffari, M. EghbaliArani, J. Amighian, J. Magn. Magn. Mater. 21 (2010) 3240-3244.
[19] H.R. Pouretedal, M. Fallahgar, F. Sotoudeh Pourhasan, M. Nasiri, Iran. J. Catal. 7 (2017) 317-326.
[20] H. Derikvandi, A. Nezamzadeh-Ejhieh, J. Hazard. Mater. 321 (2017) 629–638.
[21] M. Karimi-Shamsabadi, M. Behpour, A. Kazemi, Babaheidari, Z. Saberi, J. Photochem. Photobiol. A 346 (2017) 133-143.
[22] M. Babaahamdi-Milani, A. Nezamzadeh-Ejhieh, J. Hazard. Mater. 318 (2016) 291-301.
[23] A. Sobhani-Nasab, M. Maddahfar, S.M. Hosseinpour-Mashkani, J. Mol. Liq. 216 (2016) 1-5.
[24] M. Enhessari, A. Salehabadi, K. Maarofian, S. Khanahmadzadeh, Int. J. Bio-Inorg. Hybr. Nanomater. 5 (2016) 115-120.
[25] L. Shabani, H. Aliyan, Iran. J. Catal. 6 (2016) 221-228.
[26] L. Vafayi, S. Gharibe, Iran. J. Catal. 5 (2015) 365-371.
[27] A, Nezamzadeh-Ejhieh, M. Karimi-Shamsabadi, Chem. Eng. J. 228 (2013) 631-641.
[28] A. Nezamzadeh-Ejhieh, M. Karimi-Shamsabadi, Appl. Catal. A 477 (2014) 83-92.
[29] A. Nezamzadeh-Ejhieh, N. Moazzeni, J. Ind. Eng. Chem. 19 (2013) 1433-1442.
[30] A. Nezamzadeh-Ejhieh, S. Hushmandrad, Appl. Catal. A 388 (2010) 149-159.
[31] M.M. Jaffer Sadiq, A.S. Nesaraj, Iran. J. Catal. 4 (2014) 219-226.
[32] A. Nezamzadeh-Ejhieh, Z. Banan, Iran. J. Catal. 2 (2012) 79-83.
[33] M. Eghbali-Arani, A. Sobhani-Nasab, M. Rahimi-Nasrabadi, S. Pourmasoud, J. Electron. Mater. 47 (2018) 3757–3769.
[34] M. Eghbali-Arania, A. Sobhani-Nasabb, M. Rahimi-Nasrabadi, F. Ahmadid, S. Pourmasoud, Ultrason. Sonochem. 43 (2018) 120–135.
[35] S. Pourmasoud, A. Sobhani-Nasab, M. Behpour, M. Rahimi-Nasrabadi, F. Ahmadi, J. Mol. Struct. 1157 (2018) 607-615.
[36] S.S. Hosseinpour-Mashkani, A. Sobhani-Nasab, J. Mater. Sci. Mater Electron. 28 (2017) 16459-16466.